



**Acoustics'08  
Paris**  
June 29-July 4, 2008

[www.acoustics08-paris.org](http://www.acoustics08-paris.org)

**euonoise**

## Design of air springs for improved frequency response characteristics using computational fluid dynamics

Grace Kessenich<sup>a</sup>, Allan Pierce<sup>b</sup> and Baruch Pletner<sup>a</sup>

<sup>a</sup>IPTRADE, Inc, 1 Gateway Center Suite 601, Newton, MA 02458, USA

<sup>b</sup>College of Engineering, Boston University, 110 Cummington St, Boston, MA 02215, USA  
[grace.kessenich@iptrade.com](mailto:grace.kessenich@iptrade.com)

Large air springs can be limited in their performance as isolation devices by cavity resonances. The analysis of prototype springs with irregularly shaped cavities requires knowledge of the resonant frequencies as well as the frequency response over all frequencies of interest. Computational fluid dynamics (CFD) simulations can provide such knowledge, including phase. The simulation is unaffected by ambient noise and sensor sensitivity, major experimental concerns with such a highly isolated system. Unlike analytical methods, complex geometries can be modeled. The methodology is illustrated in the present talk with three different chambers in 2D and 3D. A chamber wall section, representing a piston, is moved at a sinusoidal displacement with constant frequency. Measurement of the magnitude and phase from the resulting sinusoidal force on this surface provides one point of a bode plot. Many simulations are run, each at a different frequency. The null and resonant frequencies are readily apparent. Comparison with analytical predictions for simple geometries validates this technique. The influence of inserted porous membranes on the frequency response is explored. Simulations provide information to design appropriate membranes and their placement within the cavity, substantially increasing the range of frequencies over which the air spring has acceptable behavior.

## 1 Introduction

High precision air springs must carry large loads and must have low spring-mass resonant frequencies, and thus low spring constants. A low spring constant requires a large air chamber. As an air chamber increases in size, it has lower resonant and null acoustic frequencies, which may be low enough to be in the control band of a typical control system (e.g. a stabilization system preventing the air spring piston from moving in the  $x$  or  $y$  direction as it moves up and down in  $z$ ). It is important to understand the location of the acoustic resonant frequencies during the design process. CFD simulations can provide this information, even for geometries that are too complicated for analytical models.

Membranes can be added to the geometries to increase the resonant frequencies without appreciably affecting the low spring constant. At low velocities or frequencies, the air can easily pass through the membrane. At high frequencies, the membrane acts as a rigid wall and effectively makes the chamber smaller, increasing the resonant frequencies. The membrane has to be designed correctly, so that the piston amplitude response remains at the static value for a wide frequency range.

## 2 Theory

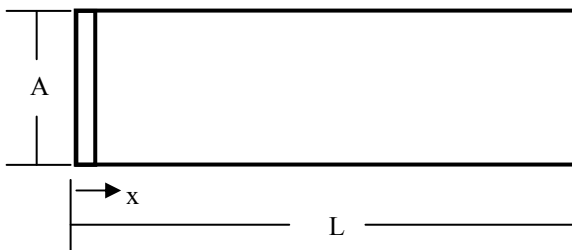


Figure 1: Simple cylinder with piston end cap

Consider a simple cylinder (shown in Figure 1) of length  $L$  with a piston of area  $A$  moving sinusoidally at  $x=0$  with an amplitude (peak displacement) of  $D$ . The cylinder is filled with a fluid that has a density  $\rho$  and speed of sound  $c$ .

The pressure in the cylinder due to the moving piston is a function of both the spatial position and the time.

$$P' = \text{Re} \left[ \hat{p}(x) e^{-i\omega t} \right] \quad (1)$$

Substituting Eq.(1) into the wave equation gives the Helmholtz Equation.

$$\frac{d^2 \hat{p}}{dx^2} + \frac{\omega^2}{c^2} \hat{p} = 0 \quad (2)$$

The simplest solution to this ordinary differential equation is

$$\hat{p} = A \cos\left(\frac{\omega}{c} x\right) + B \sin\left(\frac{\omega}{c} x\right) \quad (3)$$

There are two unknowns in this equation,  $A$  and  $B$ . To solve for them, boundary conditions must be used. The displacement of the air in the cylinder is

$$\xi = \text{Re} \left[ \hat{\xi}(x) e^{-i\omega t} \right] \quad (4)$$

Euler's equation relates this to pressure.

$$\rho_o \omega^2 \hat{\xi}(x) = \frac{d\hat{p}}{dx} \quad (5)$$

At the end wall ( $x=L$ ), the air does not move. At the piston end ( $x=0$ ), the air moves with the piston, which has an amplitude  $D$ . This gives the boundary conditions:

$$\frac{d\hat{p}}{dx} = \rho_o \omega^2 D \quad \text{at } x=0 \quad (6)$$

$$\frac{d\hat{p}}{dx} = 0 \quad \text{at } x=L$$

This gives  $A$  &  $B$  as:

$$A = B \frac{\cos\left(\frac{\omega}{c} L\right)}{\sin\left(\frac{\omega}{c} L\right)} = \frac{c \rho_o \omega D}{\tan\left(\frac{\omega}{c} L\right)} \quad (7)$$

$$B = c \rho_o \omega D$$

The pressure in the cylinder is:

$$P' = \left[ \frac{c \rho_o \omega D}{\tan\left(\frac{\omega}{c} L\right)} \cos\left(\frac{\omega}{c} x\right) + c \rho_o \omega D \sin\left(\frac{\omega}{c} x\right) \right] \cos(\omega t) \quad (8)$$

The force on the piston ( $x=0$ ) from the air when the piston is fully down ( $\cos(\omega t) = 1$ ) is:

$$F_{piston} = \frac{c \rho_o \omega D A}{\tan\left(\frac{\omega}{c} L\right)} \quad (9)$$

There are three characteristic features to note with regards to this equation: quasi-static approximation, resonant

frequency, and null frequency. The quasi-static approximation of the force is found when  $\omega$  is near 0. This results in a force of  $\rho c^2 A / L D$ . The spring constant for such a system is  $\rho c^2 A / L$ , equivalent to  $\gamma P A^2 / V$ . The resonant frequency occurs when the denominator goes to zero, or  $\tan(\omega L / c) = 0$ . The lowest non-zero frequency at which this occurs is when  $\omega L / c = \pi$ , or  $f = c / 2L$ . A null (i.e. no reaction force with a sinusoidal displacement of a certain frequency) will occur when the denominator goes to infinity. This occurs when  $\omega L / c = \pi/2$ , or  $f = c / 4L$ .

Adding a porous membrane to the chamber affects the system in two ways. First, damping is added, which causes the phase to rise more slowly, making the system significantly easier to control. Second, the effective chamber size is reduced as a function of frequency. At low frequencies, the entire chamber will participate in the system. At high frequencies the porous membrane acts as a wall, causing only part of the chamber to participate.

A dimensionless constant can be defined:  $k = \frac{c\rho}{\alpha\mu d}$ , where  $\alpha$  is the membrane resistance,  $c$  is the speed of sound,  $\rho$  is the density of the air,  $\mu$  is the viscosity, and  $d$  is the thickness of the membrane.

### 3 Representative Geometries

Three representative geometries of increasing complexity were considered. The first is a simple cylinder and was modelled only in 2D. The second is a square spring with a protruding circular piston, a mid-plane slice of which is shown in Figure 2; this is modelled in 2D and in 3D and is compared analytically to a cylinder with the area of the piston and the height of the chamber to the upper piston level. The third is a complex geometry modelled in both 2D and 3D; Figure 2 shows the 2D geometry.

In later simulations, membranes were added to these geometries at the dashed locations. The pistons, shown in dark black lines, move in the direction indicated. The membrane resistance,  $\alpha$ , is varied in the simulations, with all other variables held constant giving a variety of  $k$  values.

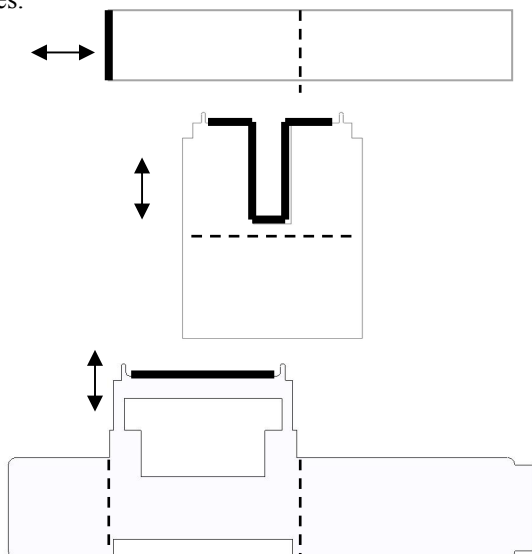


Figure 2: The three geometries considered: geometry #1, geometry #2, and geometry #3.

## 4 Analysis Procedure

The CFD software package FLUENT ([www.fluent.com](http://www.fluent.com)) is used to simulate the laminar, time-varying flow by finite volume solution of the unsteady Navier-Stokes equation. The solution procedure uses the SIMPLEC (Semi-Implicit method for Pressure Linked Equations – Consistent) algorithm for pressure-velocity coupling and the pressure discretization is based on the PRESTO! scheme. The density and momentum are computed by the second order upwind scheme which provides second order accuracy to the solution. Gravity was taken into account during the simulation, with the downward direction being so that the piston was on the upper side of the configuration. The fluid was air and was regarded as an ideal gas. Thermal conduction was taken into account with the fluid being assumed to be isothermal. The solution was considered to have converged when the error residuals were reduced below four orders of magnitude from their maximum values.

The oscillating velocity of the piston was prescribed to be  $v = A 2\pi f \cos(2\pi f t)$ , where  $A$  is the amplitude and is 0.1mm.  $t$  refers to the time step.  $f$  is the oscillation frequency. This equation gives a piston displacement of  $A \sin(2\pi f t)$ . A variety of simulations are performed, each at a different frequency. The simulation time step was set so that each cycle had 100 time steps.

The force on the piston is reported for each time step. A sine is fit to the steady state portion of the force and is compared to the input displacement in both amplitude and phase. Each simulation produces one point on a Bode plot.

## 5 Simulation Results

### 5.1 Geometry #1

To illustrate how CFD techniques can be applied, a simple example is considered for which analytical results are available, this being a simple cylinder. Three sets of simulations were run in 2D for the cylinder geometry: no membrane, a weak membrane ( $5e9m^{-2}$ ,  $k = 0.2$ ), and a strong membrane ( $1e10m^{-2}$ ,  $k = 0.4$ ). Figure 3 shows the Bode plot of the force on the piston as a function of frequency for each of the two membranes along with the no-membrane case.

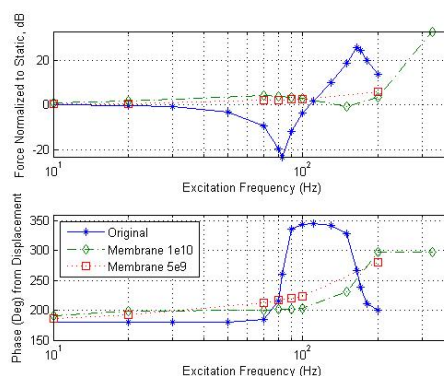


Figure 3: Bode plot of force on piston as a function of frequency, for two different membranes and no membrane

The simulation accurately predicts the null frequency of 82Hz and the resonant frequency of 165Hz.

The membranes contribute substantially to the design goal of raising the resonant frequencies outside of the range in which the system is intended to operate as a linear spring. The phase is smoother and higher for a broader frequency range, with the stronger membrane exhibiting this behavior more markedly. The first null frequency is about double for the system with the membranes compared to the system without. The effective chamber size appears to be changing with frequency when the membrane is present.

Figure 4 shows the velocity as a function of the location along the center of the cylinder for all three systems at three different frequencies: 10Hz, 100Hz, and 200Hz: 10Hz is below the null frequency for all three systems; 100Hz is between the null and resonant frequencies for the no-membrane system and below the null frequency for the membrane systems; and, 200Hz is after the resonance for the no-membrane system and is between the null and resonance frequencies for the membrane systems.

The three systems show little difference at 10Hz, with the highest deviation shown for the strongest membrane. At 100Hz, the membranes keep the velocity of those systems roughly linear between the wall and the membrane. The sinusoidal behavior only begins to occur above the membrane. At 200Hz, the velocity is negative in the chamber even as the piston velocity is positive for the original system but not for the system with the membranes.

The velocity figures show further evidence that the membranes are reducing the effective size of the chamber at the upper frequencies.

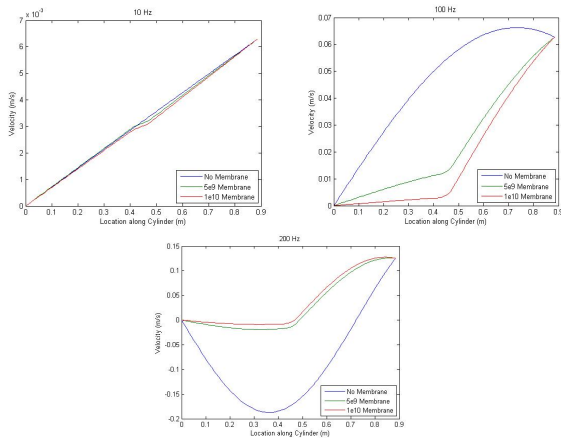


Figure 4: Velocity as function of location in chamber, for the two membranes and for no membrane, at 10Hz, 100Hz, and 200Hz

## 5.2 Geometry #2

Figure 5 shows the response of Geometry 1 as found by 2D and 3D simulations. These results match the analytical theory, which showed first null, first resonant, and second null frequencies of 262Hz, 524Hz, and 786 Hz, respectively. The differences between the 2D and 3D results can be attributed to different areas of the protruding part of the piston in 2D and in 3D. Figure 6 shows the resonant and null frequencies of: (i) the analysis assuming a cylinder, (ii) the 2D simulations, and (iii) the 3D simulations.

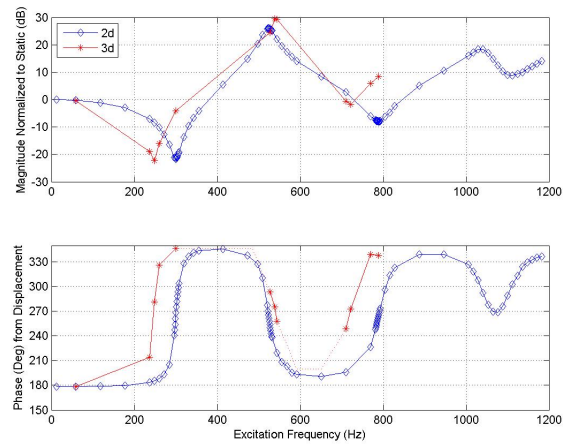


Figure 5: Frequency response of geometry #2 as found by 2D and 3D simulations

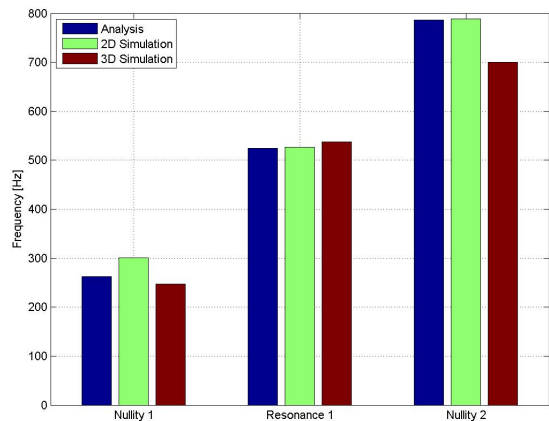


Figure 6: Analytical, 2D simulation, and 3D simulation results

Figure 7 shows the pressure in the chamber as a function of the location along a vertical line halfway between the piston and the edge of the chamber, for (i) the analysis assuming a cylinder, (ii) the 2D simulations, and (iii) the 3D simulations. Each line on the graph corresponds to a different time step for one sinusoidal cycle. The zero pressure values do not occur exactly at the piston (first nullity), halfway along the chamber (first resonance), or a third of the distance along the chamber (second nullity), because the piston protrusion into the center of the chamber changes the overall force on the piston.

For the first nullity, the location of the smallest pressure is 301mm, which corresponds to a frequency of 287Hz.

For the resonance, the smallest pressure in the chamber occurs at 158mm. The middle of the chamber (and thus the expected smallest pressure for the resonance) is at 162mm, only 2% higher than what actually happens.

For the second nullity, the lowest pressure (first pressure node) in the chamber occurs at 103mm, and the highest (first pressure anti-node) at 235mm. For a perfect cylinder, the lowest pressure in the chamber occurs at one-third of the chamber length, or 114mm, and the highest pressure occurs at two-thirds of the chamber length, or 228mm. These are off by 10% and 3%, respectively. The second pressure node is not present inside the chamber; it is presumed that it would occur just outside the chamber.

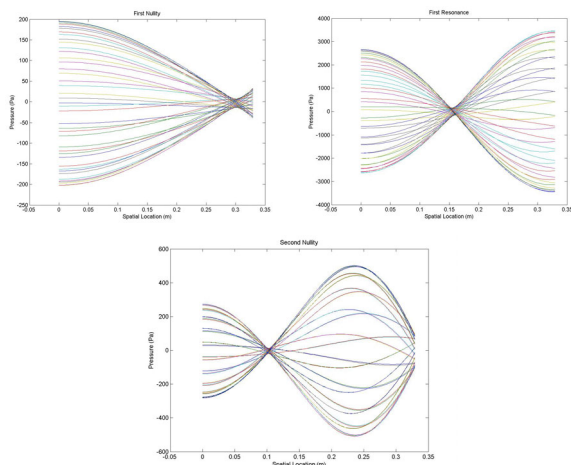


Figure 7: Pressure as a function of location along a line for: (i) first nullity, (ii) first resonance, (iii) second nullity

Four membranes were used in 2D simulations. These membranes had resistances ( $1/m^2$ ) of  $2e10$ ,  $5e10$ ,  $1e11$ ,  $2e11$ . Figure 8 shows the magnitude and phase results for all four membranes, as well as the original case.

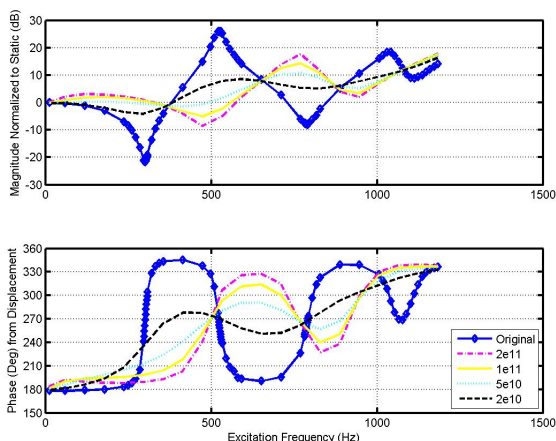


Figure 8: Frequency response of geometry #2 with and without porous membranes, from 2D simulations

These results show significant improvement in frequency response over the unmodified chamber. One recognizes three categories: membrane too weak ( $2e10m^{-2}$ ), membrane too strong ( $1e11m^{-2}$ ,  $2e11m^{-2}$ ) and membrane about right ( $5e10m^{-2}$ ).

For the weak membrane ( $2e10m^{-2}$ ), the force decreases at low frequencies, as in the original system. The resonance frequencies remain at their original values. This system is more damped than the original but nullities still occur.

For the strong membranes ( $1e11m^{-2}$ ,  $2e11m^{-2}$ ) and the about-right membrane ( $5e10m^{-2}$ ), the forces at low frequencies increase, unlike what occurs in the original system. The stronger the membrane is, the higher the slope is at low frequencies. The resonant/null frequencies are increased to the values expected for a chamber whose volume is that of the air above the membrane. The system has a higher magnitude when the membrane is stronger, as if there were less damping with the stronger membrane. These observations all lead to the conclusion that the membrane behaves more like a rigid wall than a damper at these higher frequencies.

For the about-right membrane ( $5e10m^{-2}$ ), the initial force stays constant (within 2dB) until 500Hz, compared to

150Hz in the original system. The nullities and resonances exhibit the most damping of any of the membranes and have the lowest overall magnitude. The  $k$  value is approximately 0.2.

Two additional sets of 3D simulations have been performed, one with a weak membrane ( $5e10m^{-2}$ ) and one with a strong membrane ( $2e11m^{-2}$ ). See Figure 9.

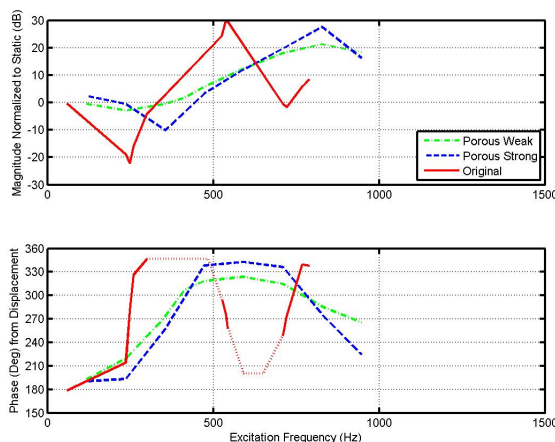


Figure 9: 3D Results with original, weak ( $5e10m^{-2}$ ), and strong ( $2e11m^{-2}$ ) membranes

Both the strong and weak membrane add damping to the system, effectively lowering the first null frequency and pushing the first resonant frequency higher. These findings correspond with the 2D results.

In 3D, the  $5e10m^{-2}$  (weak) membrane reduces the first nullity but does not move it, the latter of which happened in 2D. In the 3D simulations the membrane was not of uniform thickness due to the unstructured nature of the simulation grid. The 2D grid was structured, and its porous membrane had a uniform thickness.

Figure 10 shows the results from 2D and 3D, each with a strong ( $2e11m^2$ ) and a weak ( $5e10m^2$ ) membrane. Note that the location of the nullity is different in 2D and 3D because of the different areas of the piston protrusion. b

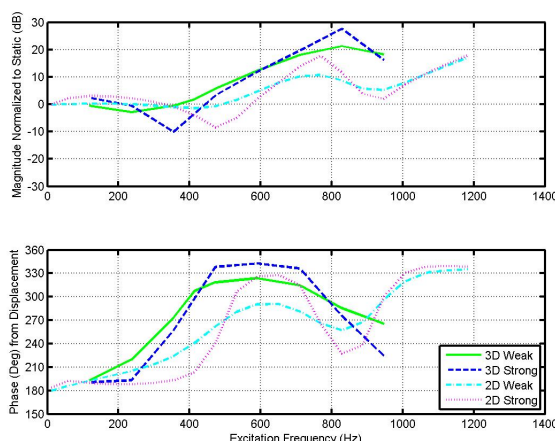


Figure 10: Porous results, 2D & 3D membranes, weak ( $5e10m^{-2}$ ) & strong ( $2e11 m^{-2}$ )

A membrane with uniform thickness and resistance near  $5e10m^{-2}$  is best for a 5mm thick membrane. This corresponds to a  $k$  value of 0.2. Figure 11 shows results of the systems without a membrane and with the best membrane, for the 2D and 3D simulations.

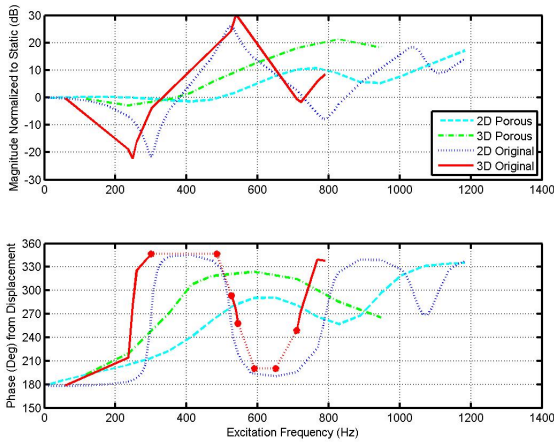


Figure 11: Original and porous (5e10) results, 2D and 3D

### 5.3 Geometry #3

Figure 12 shows the frequency response from 10Hz to 1000Hz for geometry #3 using both 2D and 3D simulations.

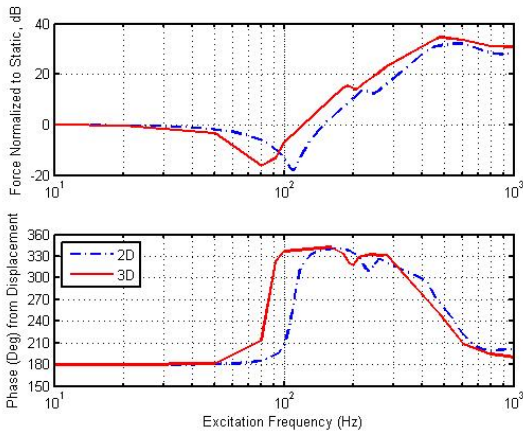


Figure 12: Simulation results from geometry #3, 2D and 3D

The 2D and 3D results match well. The first nullity is at 110Hz and the second at 249Hz. The first resonance is at 224Hz and the second at 450Hz. The effective length of a cylinder approximation can be found using  $f = m \frac{c}{L}$ , for appropriate values of the integer ratio  $m$ . Three of the four values agree within 3%.

Table 1 shows the frequency values and characteristic chamber lengths. Three of the four values agree within 3%.

Table 1: Effective chamber length of geometry #3 based on frequencies from simulation

Description	Frequency (Hz)	$m$	Length (mm)
First Nullity	110	1/4	784
First Resonance	224	2/4 =1/2	770
Second Nullity	249	3/4	1039
Second Resonance	450	4/4 =1	767

There are three regimes of the system. At lower frequencies, to approximately 50Hz, the system behaves like a spring. Between approximately 50Hz and 600Hz, the system is dominated by acoustic resonance. At upper frequencies, above approximately 600Hz, the system is dominated by viscous damping due to small channels.

Figure 13 shows the results for two membranes, compared to the original system.

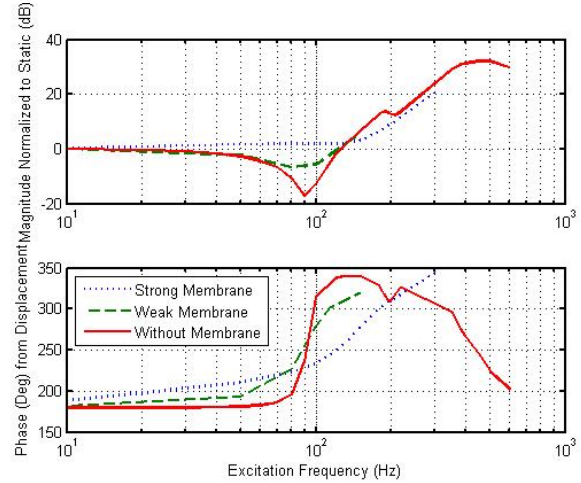


Figure 13: Simulation results comparing both membranes with the system without the membrane

The simulation results showed that the stronger membrane was the best. This configuration moved the zero frequency as well as added damping to the system. The weaker membranes simply added damping. The weak membrane corresponds with a  $k$  value of 0.2.

## 5 Conclusions

High precision air isolation devices increase isolation performance when the chamber is large. As chambers increase in size, characteristic acoustic frequencies decrease, causing problems with control systems and isolation. CFD simulations provide significant information on the behavior of a system, even with complex geometry that cannot be easily modeled analytically. Well designed membranes added to the system provide significant benefits, extending the frequency range of the static region by over 200% and decreasing the magnitude of higher resonances.